ENERGY HARVESTING FROM HYDRAULIC PRESSURE FLUCTUATIONS USING AN OSCILLATING PISTON

Hauke Lerche[1]*, Alexander Kolberg[2], Jürgen Weber[1]

[1]*Institute of Mechatronic Engineering, Technische Universität Dresden, Helmholtzstrasse 7a, 01069 Dresden*
[2] *AMR-Hydraulik Chemnitz GmbH, Nordstraße 23, 09247 Chemnitz*

* Corresponding author: Tel.: +49 351 463-33619; E-mail address: hauke.lerche@tu-dresden.de

ABSTRACT

This paper presents an analytical model of a novel energy harvester for use in hydraulic systems. The pressure pulsation caused by the pump is used as the energy source. The harvester can be connected to a hydraulic system's line and is composed of an oil volume that serves as an oil spring, a vibrating piston excited by the pressure pulsation in the hydraulic system, and an electromagnetic linear generator. The harvester is designed to be compatible with a broad static pressure range due to static pressure compensation between the oil volume and the system. The analytical description of the piston motion is derived and validated by measurements. Further, the mechanical harvester parameters are optimized to achieve maximum piston speed. Lastly, the possible performance of the harvester is estimated.

Keywords: Pressure Ripple, Autarkic Sensor

1. INTRODUCTION

The functionality of hydraulic systems, such as in sheet metal forming technology or rolling mills, is heavily dependent on sensor technology. The automated control units are based on the measured values supplied by sensors in order to manage the autonomous functional sequence of the machine. Furthermore, measurements are used to monitor and control the systems. Today's measurement technology in the field of hydraulic systems usually works with wired sensors. However, the limited flexibility in the application leads to a limited planning freedom in the positioning of the sensor, because cable guides cannot be placed everywhere. In extreme cases, especially in the industrial sector, a cable break can destroy the complete functional use of the sensor and the operation of a system may not be continued. When implementing a machine design, one must consider not only the technical risks but also the expenses for planning, materials, and cable routing. Moreover, retrofitting wired sensors can incur high costs. As an alternative, there has been a growing trend in the use of battery-operated sensors which require less effort in cabling planning and provide a higher level of safety, given the absence of cables. However, maintenance accessibility, such as for battery replacement, needs to be guaranteed, which curtails the versatility of these sensors.

In the field of research, there are already approaches for self-sufficient sensor technology through energy harvesting. Numerous publications and meta-studies [1]–[5] on the subject of energy harvesting have already been published. While many studies concern energy harvesting from vibration, some delve into energy harvesting from pressure pulsation in fluid power systems. Skow

presents a harvesting concept designed for use in hydraulic systems [6]. Here, the pressure pulsation in the fluid is transmitted to a piezostack by using a metallic diaphragm. With a pressure pulsation of 4 bar, a power output of 1.2 mW can be achieved. However, the static pressure range is restricted as the load on the piezo elements becomes excessive beyond 100 bar resulting in decreased power. To achieve higher static pressure levels the system can be preloaded, but it results in no further energy generation at low static pressure ranges. In Ren et al.'s study [7], a cylindrical magnet that is supported magnetically is excited to oscillate by pressure pulsations found in pneumatic systems. Coils near the cylinder magnet generate an induction bias. The system is stimulated with a pressure amplitude of 0.8 bar and 30 Hz, and it attains a maximum power of 2 mW.

Examining the acoustic power density of pressure pulsation (refer to **Figure 1**) [8], it is clear that the current percentage yield from pulsation is very low. This indicates the potential for optimization to increase yield.

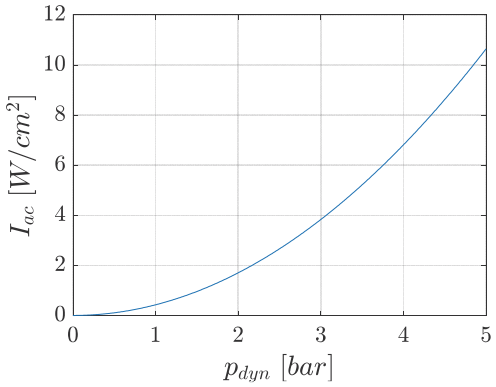

Figure 1: Acoustic Intensity of the pressure ripple in a hydraulic system

$$I_{ac} = \frac{p_0^2}{2\rho c} \tag{1}$$

2. STRUCTURE OF THE ENERGY HARVESTER

The schematic structure of the developed harvester is shown in **Figure 2**. The electromagnetic linear generator consisting of a coil and magnet is to be driven by a piston. The piston is excited to oscillation by the pressure pulsation in the system, which induces a voltage in the coil. An oil spring is to serve as the counterforce to the dynamic pulsation force of the hydraulic system. In simplified terms, the harvester can be seen as a single-mass oscillator. In order to compensate for the load caused by the static system pressure, the piston is guided in an annular gap seal through which a small volume flow can pass and thus acts as a kind of mechanical low-pass filter, whereby static pressure equalization can take place between the hydraulic system and the cavity of the harvester. The oscillation of the piston can thus be considered almost independently of the static pressure and is excited via the dynamic pressure. The influence of the static pressure on the compression modulus and the viscosity of the oil must be taken into account.

The linear generator is to provide sufficient energy for the operation of a pressure sensor as well as a radio unit. To ensure supply continuity even during standstill, a supercap will be utilized, capable of being charged by the generator as required. Nonetheless, the present study concentrates on the analytical modelling and validation of the piston oscillation.

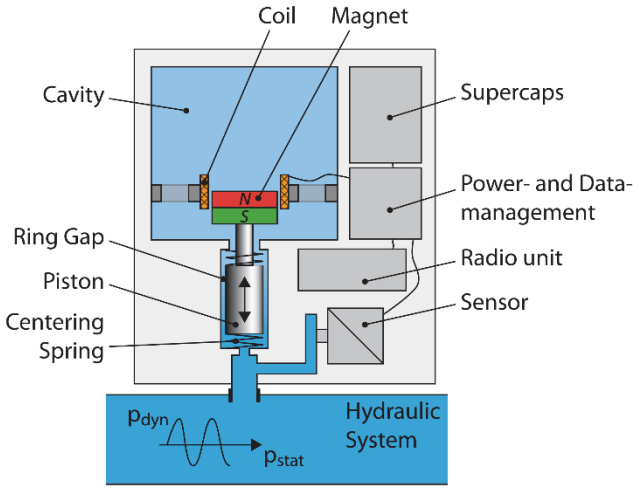

Figure 2: Schematic representation of the energy harvester

3. ANALYTICAL MODELING

The motion of the piston in the energy harvester can be described analytically on the basis of the acting forces (see **Figure 3**) using Newton's equation of motion:

$$\dot{v}(t)\, m_P + F_g + F_S - F_F + p_{Cav}(t) A_P = p_{sys}(t) A_P \tag{2}$$

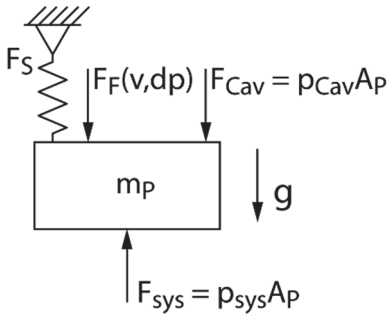

Figure 3: Forces acting on the piston of the energy harvester

Velocity and mass of the piston and the area of the piston's face are represented by v, m_P and A_P, respectively. F_F is the resultant frictional force on the piston attributed to the velocity gradient of the fluid within the annular gap. The weight force $F_g = m_P \cdot g$ and the spring force F_S of the centering springs are neglected. The pressure in the cavity p_{Cav} is denoted by the following differential equation, where the equivalent compression modulus is marked by K' and V_{Cav} represents the oil volume in the cavity:

$$\dot{p}_{Cav} = \frac{K}{V_{Cav}} (v\, A_P + Q_{Gap} + Q_{GapDrag}(v)) \tag{3}$$

The pressure gradient is determined by the speed of the piston and the volume flow through the annular gap. The drag flow $Q_{GapDrag} = 0.5 \cdot v\, A_{AnnularGap}$ caused by the piston movement can be neglected, since $A_P \ll A_{AnnularGap}$ applies. The pressure difference between system port and cavity also generates a volume flow Q_{Gap}, which can be calculated according to the following equation:

$$Q_{Gap} = \underbrace{\frac{\pi\, d_P\, s_{Gap}^3}{12\,\eta\, L_{Gap}} \left(1 + \frac{3}{2} \cdot \left(\frac{s_{exz}}{s_{Gap}}\right)^2\right)}_{=C_{Gap}} \cdot (p_{sys} - p_{Cav}) \tag{4}$$

Here, the diameter of the piston is referred to as d_P, with s_{Gap} denoting the height and L_{Gap} indicating the length of the annular gap. The dynamic viscosity of the oil is represented by η. Since the piston is not concentrically fixed in the sleeve, eccentric displacements can occur, which are taken into account by the eccentricity s_{exz}. The dynamic viscosity η is calculated as a function of the static pressure p_{stat} (in bar) [9]. For a static pressure $p_{stat} = 0\ bar$ a viscosity of $\eta_0 = 0.04\ Pa \cdot s$ is assumed.

$$\eta = \eta_0 e^{1.7 \cdot 10^{-3}\, \frac{1}{bar} p_{stat}} \tag{5}$$

To determine the frictional force, it is necessary to analyze the velocity profile v_f of the flow in the annular gap, as illustrated by **Figure 4**. It is assumed that this can be calculated from the summation of the simplified linear profile $v_{f,drag}$ due to the drag flow caused by the piston motion (see equation (6)) and the quadratic profile $v_{f,dp}$ due to the laminar flow caused by the pressure difference between the system and the cavity.

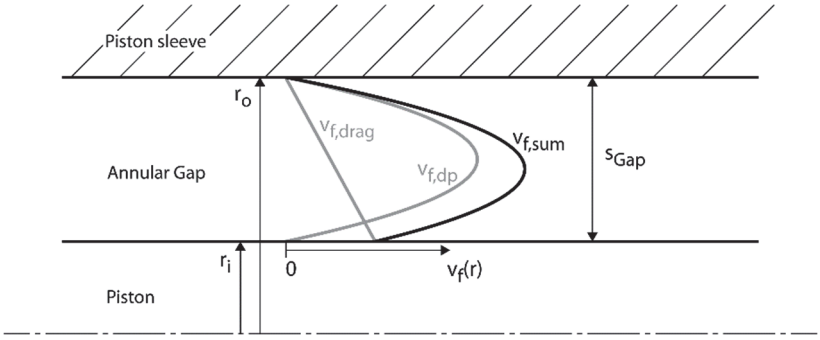

Figure 4: Velocity profiles of the fluid in the annular gap

$$v_{f,drag}(r) = -\frac{v}{r_o - r_i} r + \frac{r_a v}{r_o - r_i} \tag{6}$$

$$v_{f,dp}(r) = -\frac{6Q_{Gap}(r - r_o)(r - r_i)}{\pi(r_o - r_i)^3(r_o + r_i)} \tag{7}$$

$$v_{f,sum}(r) = v_{f,drag}(r) + v_{f,dp}(r) \tag{8}$$

Here, r_i and r_o are the inner and outer radius of the annular gap, respectively and v is the speed of the Piston. The frictional force acting on the piston can now be calculated from the velocity gradient at the point $r = r_i$ as follows, where A_{PS} is the surface area of the piston:

$$F_F = \left.\frac{dv_{f,sum}}{dr}\right|_{r=r\_i} \cdot \eta A_{PS} = \frac{6Q_{Gap}}{\pi s_{Gap}^2 (r_a + r_i)} - \frac{v}{s_{Gap}} \tag{9}$$

Substituting equations (4) and (9) into (2) and setting $r_o + r_i = r_o$, we obtain the following differential equation.

$$\left(\frac{V_{Cav}\,\ddot{p}_{Cav}}{K'} - C_{Gap}(\dot{p}_{sys} - \dot{p}_{Cav})\right)\cdot m_P + \left(\left(\frac{1}{A_P} - \frac{6}{\pi r_o s_{Gap}}\right) C_{Gap}(p_{sys} - p_{Cav}) - \frac{V_{Cav}\,\dot{p}_{Cav}}{K'}\right)\frac{\eta A_{PS}}{s_{Gap}} + p_{Cav}A_P^2 = p_{sys}A_P^2 \qquad (10)$$

Laplace transformation can be used to solve the equation in the image domain and form the transfer functions $G_p(s)$.

$$B_1 = \pi r_o A_P^2 s_{Gap}^2 + 6A_{PS}C_{Gap}A_P\eta - \pi A_{PS}C_{Gap}r_o s_{Gap}\eta \qquad (11)$$

$$G_p(s) = \frac{\hat{p}_{Kav}(s)}{\hat{p}_{sys}(s)} = \frac{\frac{\pi C_{Gap}m_P r_o s_{Gap}^2}{B_1}s + 1}{\frac{\pi V_{Cav}m_P r_o s_{Gap}^2}{K'B_1}s^2 + \frac{\pi r_o s_{Gap}(C_{Gap}m_P K' s_{Gap} + A_{PS}V_{Cav}\eta)}{K'B_1}s + 1} \qquad (12)$$

In addition, the transfer function $G_v(s)$ is required. From equations (3) and (4), the following equation can be generated after reshaping and transformation into the image domain.

$$s\hat{p}_{Cav}(s) = \frac{K'}{V_{Cav}}(\hat{v}\,(s)A_P + C_{Gap}(\hat{p}_{sys}(s) - \hat{p}_{Cav}(s))) \qquad (13)$$

If this is converted to p_{Cav} and inserted into the Laplace Transform equation (2), the transfer function $G_v(s)$ can be calculated:

$$G_v(s) = \frac{\hat{v}(s)}{\hat{p}_{sys}(s)} = \frac{\overbrace{\frac{V_{Cav}(\pi A_P r_o s_{Gap}^2 + 6A_{PS}C_{Gap}\eta)}{K'B_1}}^{=T_D}s}{\underbrace{\frac{\pi V_{Cav}m_P r_o s_{Gap}^2}{K'B_1}}_{=T_1^2}s^2 + \underbrace{\frac{\pi r_o s_{Gap}(C_{Gap}m_P K' s_{Gap} + A_{PS}V_{Cav}\eta)}{K'B_1}}_{=2DT_1}s + 1} \qquad (14)$$

It can be seen that the transfer function $G_v(s)$ corresponds to a DT2 term. Consequently, the time constants T_1 and T_D can be represented as in equation (14) and the damping D can be calculated as follows:

$$D = \frac{\pi r_o s_{Gap}(C_{Gap}m_P K' s_{Gap} + A_{PS}V_{Cav}\eta)}{2\sqrt{\frac{B_1\pi V_{Cav}m_P r_o s_{Gap}^2}{K'}}} \qquad (15)$$

In contrast to a conventional single-mass oscillator, another factor that affects the damping occurs here in addition to the friction in the annular gap, namely the volume flow through the annular gap.

4. EXPERIMENTAL STUDIES

The validation and parameter identification of the system equations is carried out by means of high-frequency pressure measurements on a demonstrator (see **Figure 6**). Since only the behavior of the piston oscillation is to be investigated here, no linear generator is used in this setup. However, placeholder masses can be attached to the piston rod. In addition, the cavity is designed in such a way that the volume can be variably adjusted. The demonstrator is installed in a simple hydraulic circuit as shown in **Figure 6** below, and the pulsation of the system and cavity pressure can be measured. To avoid falsification of the measured values due to reflections and standing waves in the system, the system pressure is measured as close as possible to the energy harvester. If the system pressure is

recorded too far away, the error between the measured value and the true dynamic pressure p_{sys} at the input of the harvester - which is used in the analytical calculation - is too large. For the validation, different static pressure ranges from 50 bar to 200 bar were investigated.

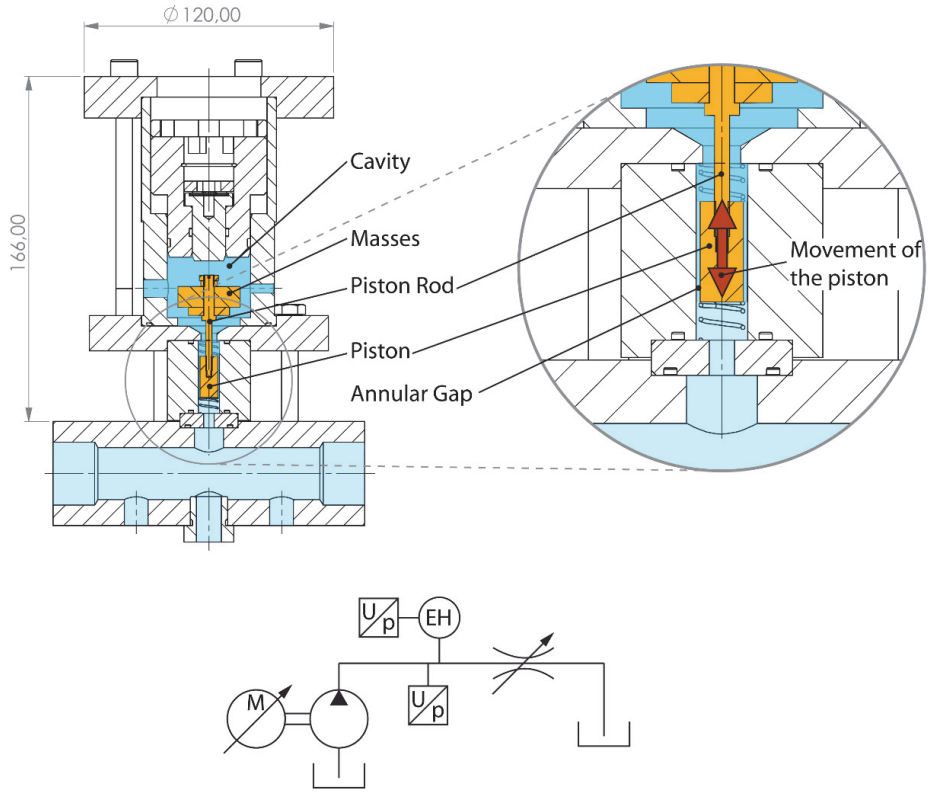

Figure 6: Mechanical structure of the demonstrator (top) and simplified hydraulic circuit diagram of the measurement setup (bottom) (EH...Energy Harvester)

Figure 5 illustrates the time dependent curve and the frequency spectrum of the system pressure and the cavity pressure at a speed of 1500 rpm. As expected, the fundamental frequency of 225 Hz corresponds to the speed of the axial piston pump multiplied by the number of pistons. In addition, several harmonic vibrations occur. Their characteristics depend, among other things, on the structure of the hydraulic system, since reflections and thus standing waves occur. These can be suppressed by the use of a RALAs [10]. Since the pulsation of the system pressure is recorded directly at the energy

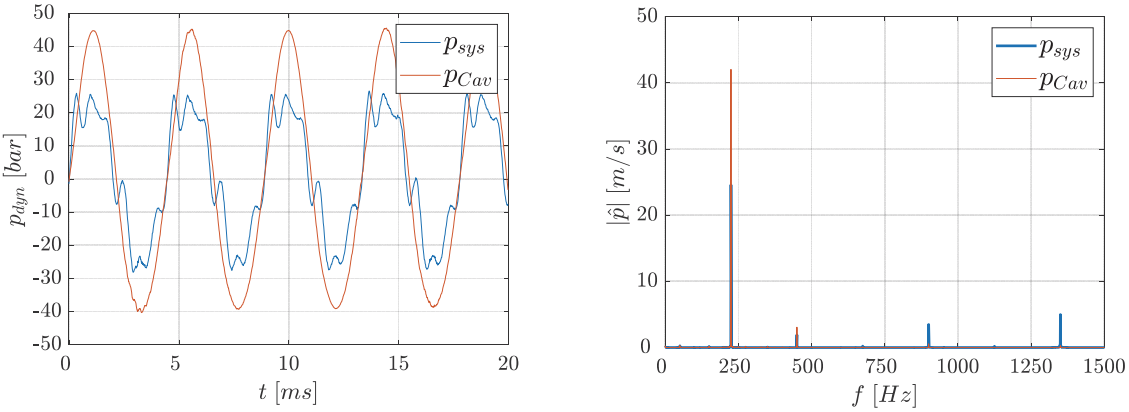

Figure 5: Time dependent curve (left) and frequency spectrum (right) of the dynamic pressure in the system and in the cavity of the Harvester at a pump speed of 1500 rpm and a static pressure of 150 bar. Parameters: $V_{Cav} = 40.9\ cm^3$, $m_P = 0.046\ kg$, $s_{Gap} = 0.08\ mm$, $d_P = 10\ mm$

harvester and the relationship between system and cavity pressure is considered for the validation, the reflection of the pressure waves has no influence on the basic measurements for investigating the behavior of the harvester. Therefore, the use of a RALA is not necessary.

The measurement data can be used to create a transfer function by analyzing the frequency and phase spectra of both the system and cavity pressure. For this purpose, the ratio of the amplitudes and phases of the system pressure at the five harmonics to those of the cavity pressure at identical frequency is determined. In this way, a Bode chart is created based on measurements at different pump speeds. **Figure 7** shows this for the case of a static pressure at 150 bar, a cavity volume of 40.9 cm³, a piston mass of 46 g and an annular gap height of 0.08 mm. Also shown in the diagram is the curve of the analytical transfer function. This was fitted to the measured data on the basis of the phase curve in order to determine the equivalent compression modulus K' and the eccentricity of the piston s_{exz}. It can be seen that the behavior of the harvester can be reproduced in wide ranges by the linear transfer function. Above the natural frequency, however, deviations occur due to nonlinear effects.

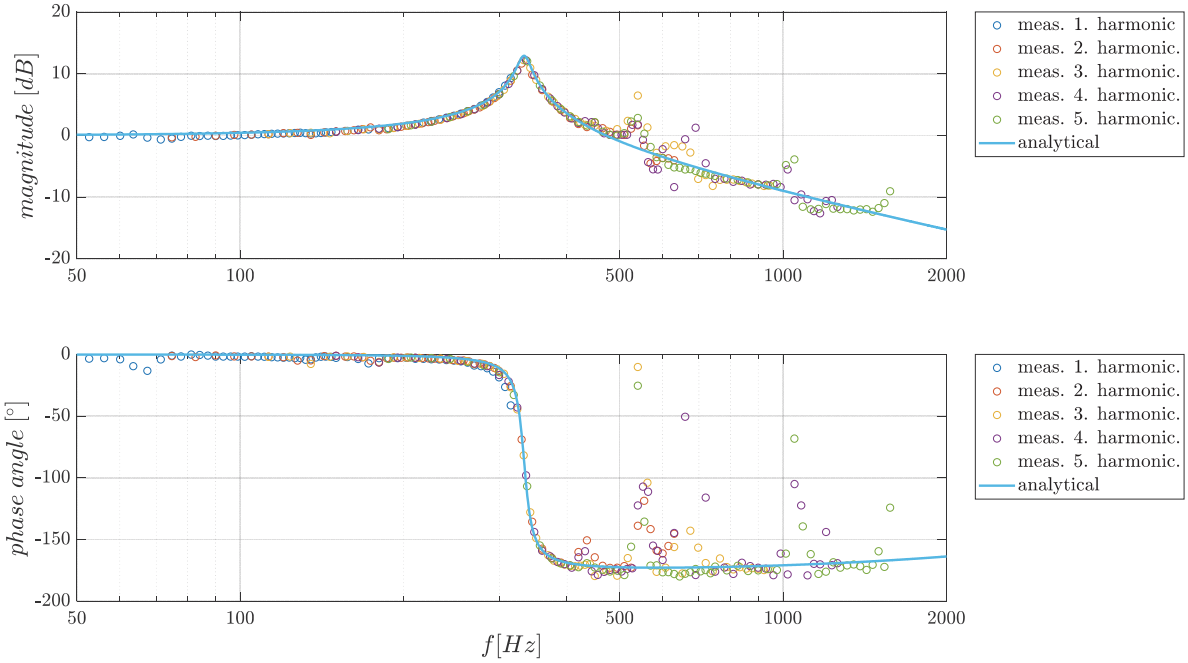

Figure 7: Experimentally and analytically determined Bode chart of $G_v(s)$ at a static pressure of 150 bar.
Parameters: $V_{Cav} = 40.9\ cm^3$, $m_P = 0.046\ kg$, $s_{Gap} = 0.08\ mm$, $d_P = 10\ mm$

In the range of the natural frequency of the demonstrator, there is an approximately 16-fold increase in the system pulsation, or an increase of 12 dB. This means that with an assumed pulsation amplitude in the system of 10 bar, the pressure in the cavity pulsates at 160 bar. However, only higher harmonics of the pressure pulsation were employed in experimental measurements to stimulate the resonant frequency, which led to the cavity pressure not achieving such high absolute pulsation. At high-pressure pulsations and correspondingly high piston velocities, there may be damping effects that are not considered analytically, for instance, caused by cavitation in the cavity.

To ensure that the analytical model is also valid at other operating points, additional measurements were carried out with varying parameters. **Table 1** shows the results for these measurements. Using the parameters K' and s_{exz} determined from the fitting function, the time constants T_1 and T_D as well as the damping D of the transfer function $G_p(s)$ can be calculated. The experimentally determined parameters K' and s_{exz} as well as the resulting damping with respect to the static pressure are shown in **Figure 8**.

Table 1: Parameters of the demonstrator an the transfer function at different measurements

meas	mP [g]	sGap [mm]	VCav [cm³]	T1 [ms] (pstat=150bar)	TD [ms] (pstat=150bar)	D (pstat=150bar)
1	46	0,08	40,9	0,477	0,022	0,0256
2	46	0,08	37,6	0,453	0,023	0,0268
3	16	0,08	46,3	0,307	0,008	0,0166
4	16	0,08	41,3	0,300	0,008	0,0169
5	16	0,13	46,3	0,309	0,019	0,0328
6	16	0,13	41,3	0,300	0,019	0,0348

The left side of **Figure 8** displays the changes observed in the equivalent compression modulus regarding static pressure for various harvester configurations. The outcomes show substantial fluctuations between measurements, however, a noticeable increase in the equivalent compression modulus with an increasing static system pressure is observable. This causes a rise in the natural frequency of the harvester. The low values of the equivalent compression modulus compared to the compression moduli reported in the literature (for example, $K_{oil}(200\ bar) \approx 18500\ bar$ [9]) are due to the compliance of the bolts and seals, as well as a the presence of free air. For measurements with an annular gap height of 0.08 mm, the eccentricity is relatively constant and is just below or at the maximum value of 0.08 mm. For measurements with an annular gap height of 0.13 mm, the eccentricity fluctuates more, but does not reach the maximum value. The damping decreases slightly across the static pressure. This decrease can be attributed to the increasing viscosity and subsequent reduction in volume flow through the annular gap (compare equation (4)). The damping increases with increasing gap size, which is in line with expectations.

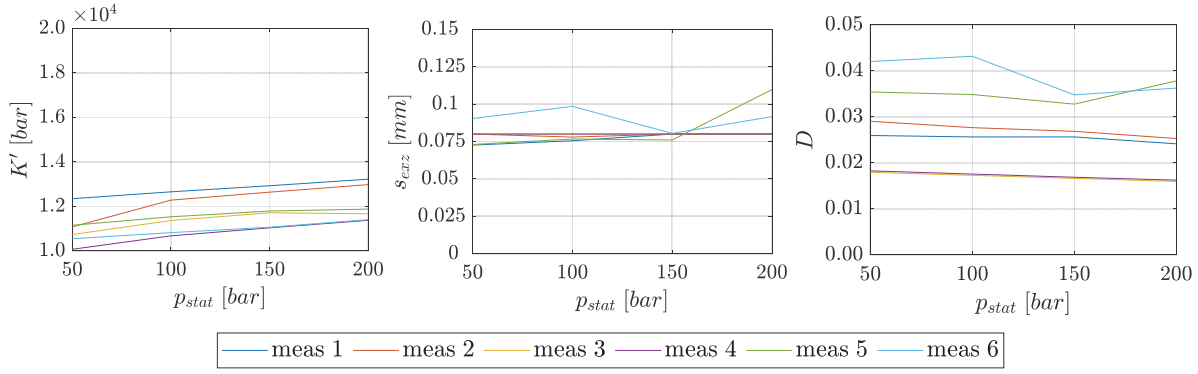

Figure 8: Parameters $K'$and s_{exz} determined using the fitting function and the resulting attenuation for different measurement setups (see **Table 1**)

Overall, it can be seen that the principle behavior of the harvester can be predicted to a large extent via the linear, analytical transfer function. This can also be shown in **Figure 9**, where the comparison between the measured values of the cavity pressure and the cavity pressures calculated via the inverse transfer function $G_p(s)$ is presented.

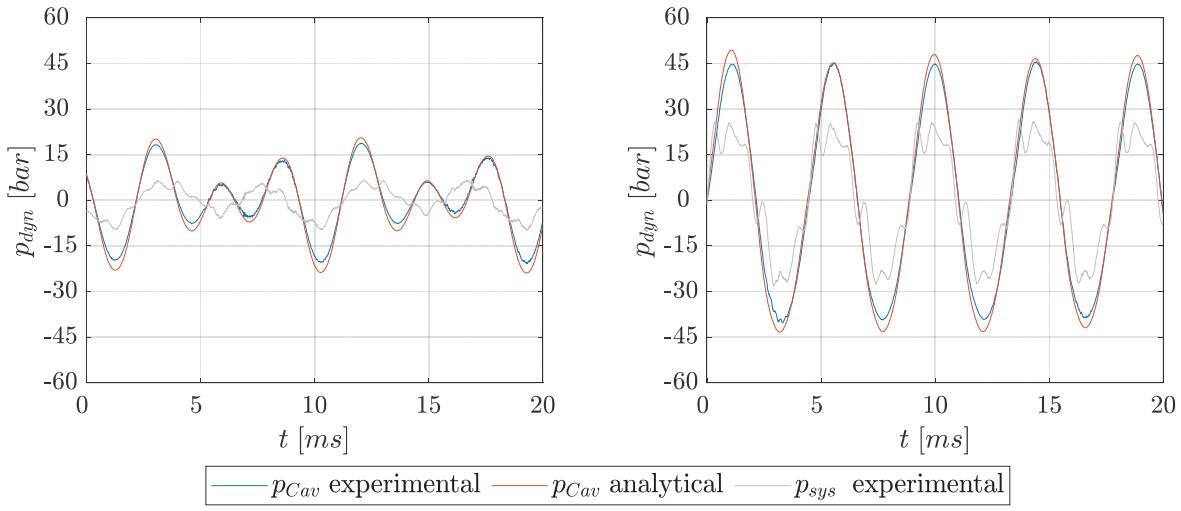

Figure 9: Comparison of the measured data and the analytical calculation of the pressure pulsation in the cavity at a pump speed of 750 rpm (left) and 1500 rpm (right)

5. OPTIMIZATION OF THE PISTON MOVEMENT

The objective of the harvester is to maximize energy extraction from pressure pulsations. An electromagnetic linear generator is implemented to induce voltage through piston movement. In a fundamental coil-solenoid combination, as shown in **Figure 2**, the induced voltage can be determined via the following equation:

$$U_{ind} = -N\frac{d\phi}{dt} = -N\frac{d\phi}{dx}\cdot\frac{dx}{dt} \tag{16}$$

Here N represents the number of turns of the coil, $d\phi/dx$ indicates the magnetic flux gradient in the direction of movement of the piston and dx/dt the piston speed. Using the induced voltage and the ohmic resistance of the coil R_C as well as the load resistance R_L, the power at the load resistance of the generator can be calculated. The inductance of the generator coil is considered negligible due to the low frequency of the piston movement (< 1 kHz).

$$P_{Last} = \frac{R_L}{(R_L + R_C)^2}\, U_{ind}^2 \tag{17}$$

The flux gradient $d\phi/dx$ is reliant on the linear generator's design, and several factors affect it, including the magnet geometry, type, number of windings, and wire diameter. However, these parameters will not be explored in greater depth in the following optimization of the mechanical components. Along with the flux gradient, the generator's performance is also influenced quadratically by the piston speed and will be optimized in the following.

In order to achieve the highest possible energy yield from the harvester, the design is to be optimized with regard to maximum piston speed. The first step is to examine the influence of the cavity volume. Inserting the resonance case, $s = j/T_1$ - which provides the highest velocity - into $G_v(s)$ produces the following equation:

$$G_v\left(s = j\frac{1}{T_1}\right) = \frac{V_{Cav}(\pi A_P r_o s_{Gap}^2 + 6A_{PS}C_{Gap}\eta)}{\pi r_o s_{Gap}(C_{Gap}m_P K' s_{Gap} + A_{PS}V_{Cav}\eta)} \tag{18}$$

As the cavity volume increases, the transfer function and consequently, the piston speed also increase.

This can be explained by the fact that the pressure gradient in the cavity, due to the annular gap volume flow, decreases as the volume increases and so does the resulting damping (refer to equation (15)). This effect becomes more pronounced with increasing annular gap. In practice, however, due to installation space limitations, the cavity volume can only be increased to a limited extent. Therefore, for the following calculations, it is assumed constant with $V_{Cav} = 40\ cm^3$.

Figure 10 shows the maximum speed of the piston as a function of the relative eccentricity of the piston and at various annular gap heights. It is observed that with low ring gaps the piston speed is almost independent of the eccentricity. However, as the ring gaps increase, the piston speed falls more precipitously in relative terms.

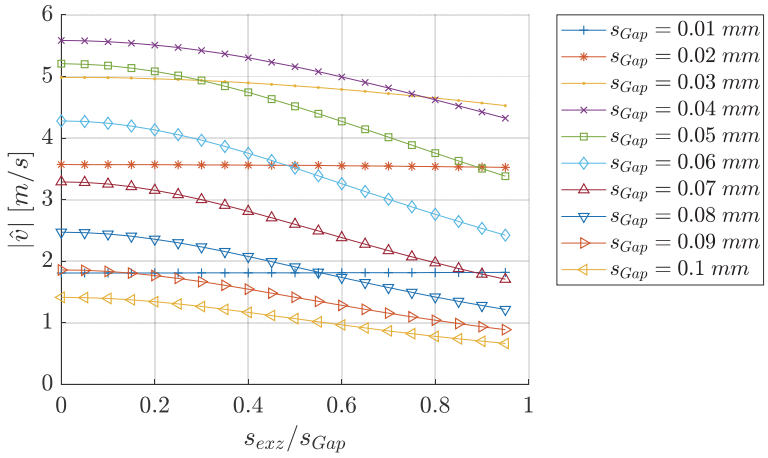

Figure 10: Maximum piston speed as a function of relative eccentricity at different ring gap heights. $m_P = 0{,}05\ kg$, $d_P = 11{,}5\ mm$, $p_{dyn} = 1\ bar$

Figure 11 depicts the behaviour of the maximum piston speed as a function of piston mass and ring gap height at maximum (left) and minimum (right) eccentricity. To ensure comparability, the natural frequency according to equation (19) is assumed to be $f_0 = 225\ Hz$, which aligns with the excitation frequency of a 9-piston pump operating at a speed of 1500 rpm. Additionally, the cavity volume ($V_{Cav} = 40\ cm^3$) remains constant. As a result, with varying piston mass, the piston diameter can be expressed as $d_P = d_P(m_P)$.

$$f_0 = \frac{1}{2\pi}\sqrt{\frac{K' A_P^2}{V_{Cav} m_P}} \approx \frac{1}{2\pi T_1} \tag{19}$$

$$d_P = \sqrt{8 f_0 \sqrt{\frac{V_{Cav} m_P}{K'}}} \tag{20}$$

Figure 11 displays that the optimal mass for the piston rises as the annular gap diminishes. Despite an increase in mass, the absolute value of the respective optimum falls only insignificantly and is just below 6 m/s at an amplitude of the system pressure of 1 bar. The small impact of the mass can be explained by the increase of the piston diameter d_P according to equation (20) alongside its mass, leading to the increase in the excitation force $F_{psys} = p_{sys}\, A_P$. The increase in excitation force can also account for the shift of the optima towards larger masses with decreasing annular gap and the consequent increase in friction. However, it is worth noting that the calculations were carried out with

certain simplifications, and the fact that a larger mass may generate a higher flow resistance under certain circumstances was not taken into consideration.

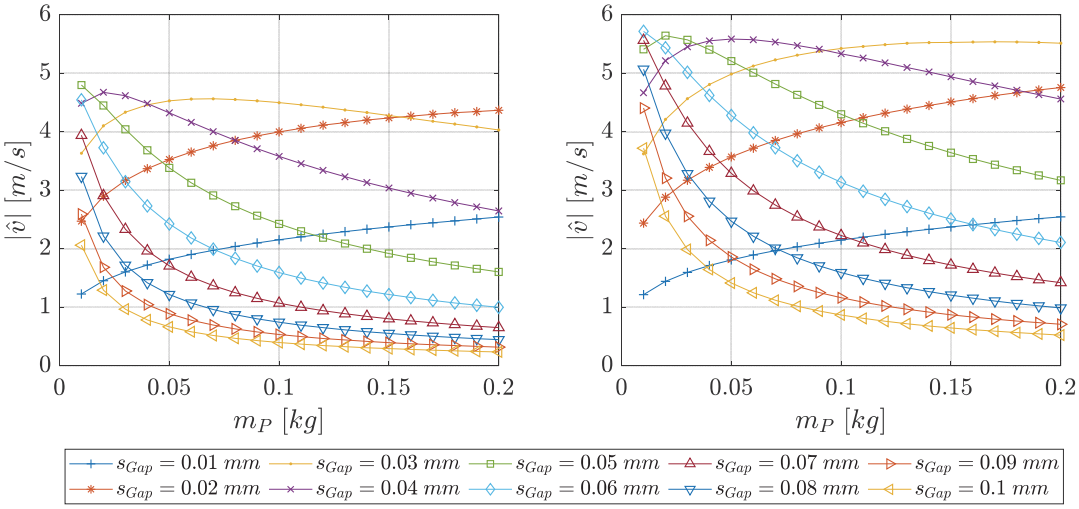

Figure 11: Maximum velocity of the piston as a function of the piston mass and the height of the annular gap at maximum (left) and minimum (right) eccentricity of the piston. Dynamic pressure amplitude of the system $p_{dyn} = 1\ bar$.

6. LINEAR GENERATOR

A linear generator composed of a cylindrical magnet and a coil is utilized to generate energy from the movement of the piston. The simple design ensures robust behaviour and low acquisition costs. The calculations in the previous section show that the maximum speed of the piston is almost independent of the mass under the given assumptions. Therefore, the cylinder magnet can be attached to the piston and the coil can be permanently installed as a stator in the harvester. This significantly simplifies the design of the linear generator and reduces its susceptibility to errors that would otherwise increase due to a moving coil.

An example to demonstrate the achievable performance of the harvester will be briefly explained here. First, the electromagnetic damping of the generator is calculated using the following equation

$$D_{em} = \frac{1}{R_L + R_c + j\omega L_c}\left(N\frac{d\phi}{dx}\right)^2 \tag{21}$$

Here, R_C refers to the ohmic coil resistance, R_L refers to the load resistance, and N signifies the number of windings. The inductance of the generator coil L_c is considered negligible due to the low frequency of the piston movement (< 1 kHz). The magnetic flux gradient $d\phi/dx$ was determined through an FEM analysis of a cylindrical magnet with a diameter of 20 mm and a height of 13 mm, using a coil with 250 turns and a wire diameter of 0.35 mm. The magnet has a mass of 0.03 kg, resulting in the piston having a total mass that corresponds with the experimental measurement of $m_P = 0.046\ kg$. The chosen example exhibits an achieved electromagnetic damping of $D_{em} = 0.21\ Ns/m$ for a load resistance of $R_L = R_C = 6.3\ \Omega$, enabling optimal utilization if D_{em}<< parasitic damping [2]. To determine the transfer function $G_{vDem}(s)$, this must be incorporated into the analytical equation of motion of the piston or linear generator.

$$B_2 = \pi r_o A_P^2 s_{Gap}^2 + 6A_P A_{PS} C_{Gap}\eta \tag{22}$$

$$B_3 = \pi D_{em} V_{Cav} r_o s_{Gap}^2 + \pi A_{PS} V_{Cav} r_o s_{Gap} \eta + \pi m_P r_o C_{Gap} K' s_{Gap}^2 \tag{23}$$

$$G_{vDem}(s) = \frac{\hat{v}(s)}{\hat{p}_{sys}(s)} = \frac{s \cdot \frac{V_{Cav}}{A_P K'} \left(1 - \frac{C_{Gap}}{V_{Cav}} \cdot \frac{B_3}{B_2}\right)}{\frac{\pi V_{Cav} m_P r_o s_{Gap}^2}{K' B_2} s^2 + \frac{B_3}{K' B_2} s + 1} \tag{24}$$

The Power $\hat{P}_{el}$ of the generator is:

$$\hat{P}_{el}(s) = D_{em} \cdot \hat{v}(s)^2 \tag{25}$$

Figure 12 displays the amplitude curve of the energy harvester's power under a pressure pulsation of 1 bar. A power of slightly over 2 W is attained at the natural frequency of 225 Hz. However, the power decreases quickly outside the resonant frequency and is only 15 mW at 200 Hz.

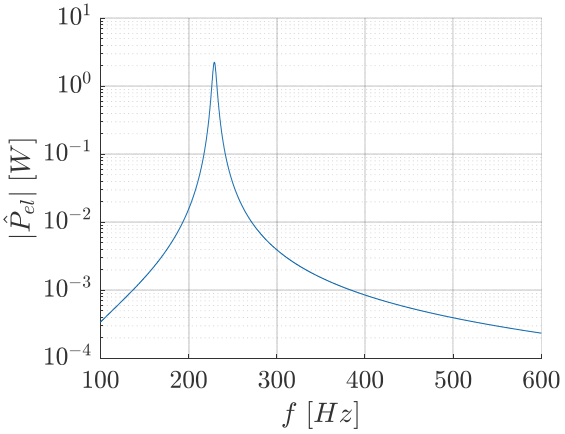

Figure 12: Magnitude plot of the generator power with the following parameters: $p_{dyn} = 1\ bar$, $V_{Cav} = 40\ cm^3$, $m_P = 0.05\ kg$, $s_{Gap} = 0.03\ mm$, $N = 250$, $d_w = 0.35mm$

7. CONCLUSION AND SUMMARY

This paper presents an analytical model for mapping the piston oscillation of a newly developed energy harvester with an electromagnetic generator. The model was validated using several measurements done on a demonstrator. Using the analytical model, it was possible to optimize the mechanical parameters of the energy harvester for maximum piston speed and the resulting high output of the generator. It was shown that the maximum piston speed depends only slightly on the mass of the oscillating piston, thus enabling a design of the linear generator with the coil as stator. Furthermore, the speed of the piston depends significantly on the height of the annular gap. The specific size of the gap depends, among other factors, on the mass of the piston and is situated at $s_{Gap} = 0.03$ mm for $m_P = 0.05\ kg$. In order to calculate the power of the generator, the analytical model was extended accordingly. At a pressure amplitude of 1 bar a power of more than 2 W could be calculated. However, since this is a resonance energy harvester, this only applies to a limited frequency range. Therefore, the application is mainly useful in systems which are driven by a pump with constant speed. Among other factors, adjusting the cavity volume can change the natural frequency of the harvester to be adapted to the specific system.
Due to the relatively low piston speed during validation, as the resonant frequency of the demonstrator was only excited by higher harmonics of the pressure pulsation, further

investigations should be made here. In this context, it must be checked whether damping effects not previously considered occur at higher piston speed. Furthermore, it is necessary to validate the entire analytical model including the linear generator on the basis of measurement data.

This Project is supported by the Federal Ministry for Economic Affairs and Climate Action (BMWK) on the basis of a decision by the German Bundestag.

NOMENCLATUR

A_P	Area of the piston's face	m²
A_{PS}	Surface area of Piston	m²
$B_{1\dots3}$	Auxiliary parameter	
C_{Gap}	Auxiliary parameter annular Gap	m³/(sPa)
D	Dampening	
D_{em}	Electromagnetic Dampening	Ns/m
d_P	Piston diameter	m
d_w	Wire diameter	m
f_0	Natural frequency	Hz
G_p	Transfer function	
G_v	Transfer function	m/(sbar)
K'	Equivalent Bulk modulus	Pa
L_c	Coil Inductance	H
m_P	Piston Mass	kg
N	Number of turns	
p_{dyn}	Dynamic Pressure	Pa
p_{stat}	Static Pressure	Pa
p_{sys}	System Pressure	Pa
p_{Cav}	Cavity Pressure	Pa
R_c, R_L	Coil, Load resistor resistance	Ohm
r_o, r_i	Outer, inner Radius annular Gap	m
s_{Gap}	Height annular Gap	m
T_1, T_D	Time constant	s
v	Piston velocity	m/s
v_f	Flow velocity	m/s
V_{Cav}	Cavity Volume	m³
η	Dynamic Viscosity	Pas
ϕ	Magnetic flux	
ν	Kinematic Viscosity	m²/s
ρ	Density	kg/m³

REFERENCES

[1] M. Ahmad und F. Khan, „Review of vibration based electromagnetic-piezoelectric hybrid energy harvesters“, *Int. J. Energy Res.*, Bd. 45, Dez. 2020, doi: 10.1002/er.6253.

[2] S. Priya und D. J. Inman, *Energy Harvesting Technologies*. New York, NY, UNITED STATES: Springer, 2008. Zugegriffen: 4. Oktober 2021. [Online]. Verfügbar unter: http://ebookcentral.proquest.com/lib/slub/detail.action?docID=417906

[3] M. Safaei, H. A. Sodano, und S. R. Anton, „A review of energy harvesting using piezoelectric materials: state-of-the-art a decade later (2008–2018)“, *Smart Mater. Struct.*, Bd. 28, Nr. 11, S. 113001, Okt. 2019, doi: 10.1088/1361-665X/ab36e4.
[4] C. Cepnik, R. Lausecker, und U. Wallrabe, „Review on Electrodynamic Energy Harvesters—A Classification Approach“, *Micromachines*, Bd. 4, S. 168–196, Juni 2013, doi: 10.3390/mi4020168.
[5] J. J. Aranda, S. Bader, und B. Oelmann, „Self-Powered Wireless Sensor Using a Pressure Fluctuation Energy Harvester“, *Sensors*, Bd. 21, Nr. 4, Art. Nr. 4, Jan. 2021, doi: 10.3390/s21041546.
[6] E. Skow, „Harvesting energy from acoustic pressure fluctuations within hydraulic systems via excitation of piezoelectric stacks“, Mai 2017. Zugegriffen: 2. August 2023. [Online]. Verfügbar unter: https://www.semanticscholar.org/paper/Harvesting-energy-from-acoustic-pressure-within-via-Skow/25508b5889d98cb4478d8a119baab22a7d7683ba
[7] H. Ren und T. Wang, „Development and modeling of an electromagnetic energy harvester from pressure fluctuations“, *Mechatronics*, Bd. 49, S. 36–45, Feb. 2018, doi: 10.1016/j.mechatronics.2017.11.008.
[8] E. Hering, R. Martin, und M. Stohrer, *Physik für Ingenieure*. Berlin, Heidelberg: Springer Berlin Heidelberg, 2021. doi: 10.1007/978-3-662-63177-5.
[9] D. Will und N. Gebhardt, Hrsg., *Hydraulik*. Berlin, Heidelberg: Springer Berlin Heidelberg, 2014. doi: 10.1007/978-3-662-44402-3.
[10] H. Theissen, „Die Berücksichtigung instationärer Rohrströmungen bei der Simlulation hydraulischer Anlagen Thiessen“, RWTH Aachen, 1983.